Supporting information

Encapsulating Si Nanoparticles in Multi-Shell Hollow Spheres: An Effective Approach to Boost the Cyclability

Huan Du[1,2], Ruohan Yu[2,3], Xingnian Tan[1], Jinsong Wu[1,3], Dongyuan Zhao[1], Liqiang Mai[1,4] and Liang Zhou[1,4*]

[1] State Key Laboratory of Advanced Technology for Materials Synthesis and Processing, Wuhan University of Technology, Wuhan 430070, China

[2] International School of Materials Science and Engineering, Wuhan University of Technology, Wuhan 430070, China

[3] Nanostructure Research Center (NRC), Wuhan University of Technology, Wuhan 430070, China

[4] Hubei Longzhong Laboratory (LZL), Wuhan University of Technoology, Xiangyang 441106, China

*Corresponding author (liangzhou@whut.edu.cn)

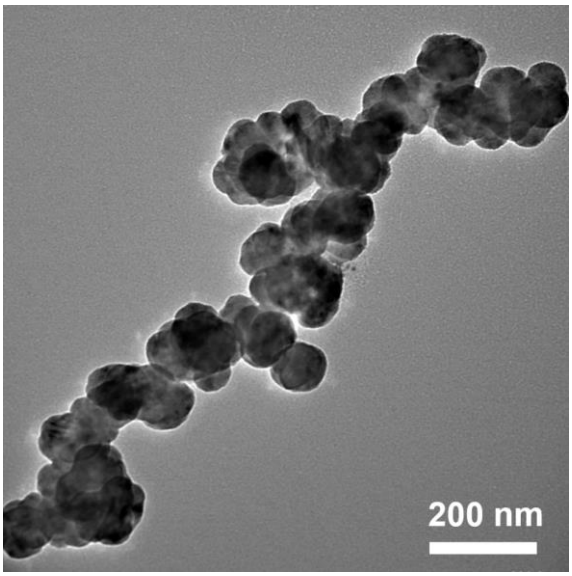

Figure S1 Morphology characterization. TEM image of the Si nanoparticles.

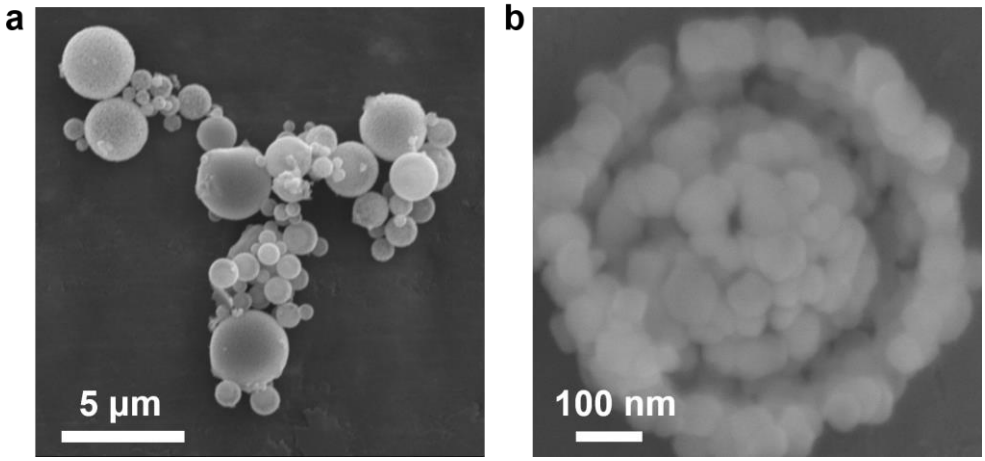

Figure S2 Morphology characterizations. SEM images of $Si/Cr_2O_3/C$ at different magnifications.

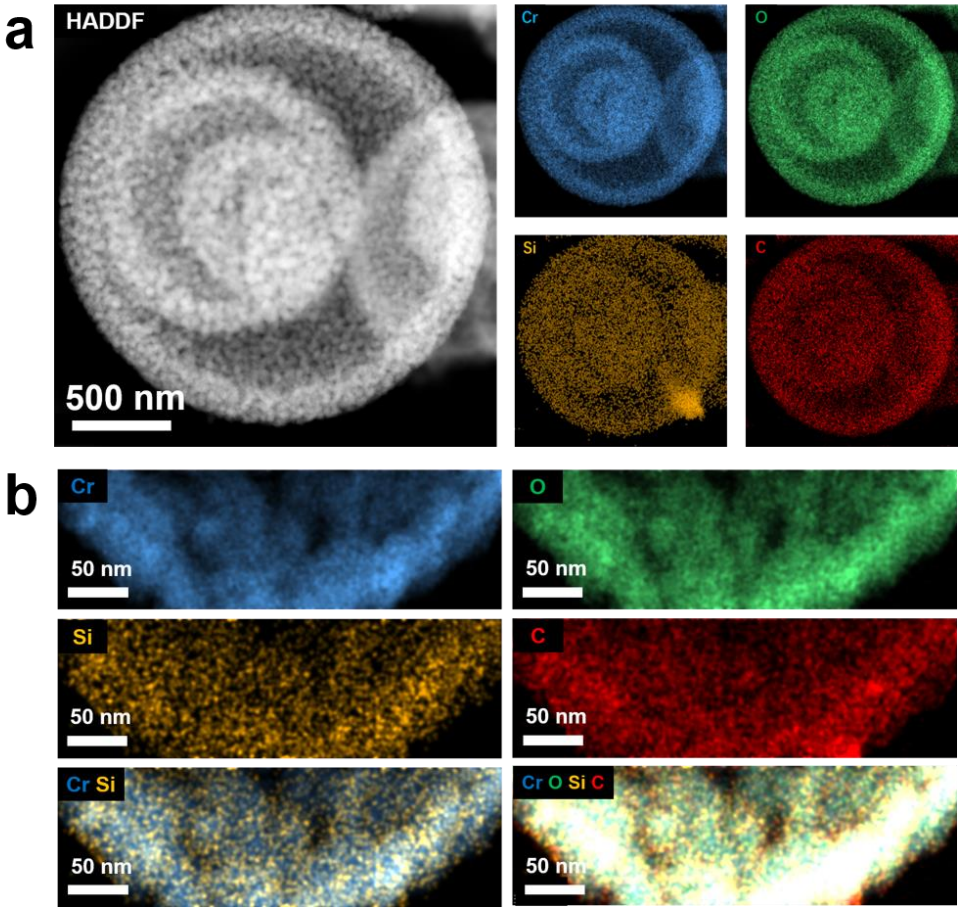

Figure S3 EDS mappings of Si/Cr_2O_3/C. STEM images and the corresponding elemental mappings of Si/Cr_2O_3/C.

Table S1. Preparation conditions for different samples.

Samples	**Si (g)**	**$Cr(NO_3)_3$ $9H_2O$ (g)**	**Sucrose (g)**
Si-0/Cr_2O_3	0	4.00	3.42
Si-0/Cr_2O_3/C	0	4.00	3.42
Si-1/Cr_2O_3	0.10	4.00	3.42
Si-1/Cr_2O_3/C	0.10	4.00	3.42
Si-2/Cr_2O_3	0.20	4.00	3.42
Si-2/Cr_2O_3/C	0.20	4.00	3.42
Si-3/Cr_2O_3	0.30	4.00	3.42
Si-3/Cr_2O_3/C	0.30	4.00	3.42
Si-4/Cr_2O_3	0.40	4.00	3.42
Si-4/Cr_2O_3/C	0.40	4.00	3.42

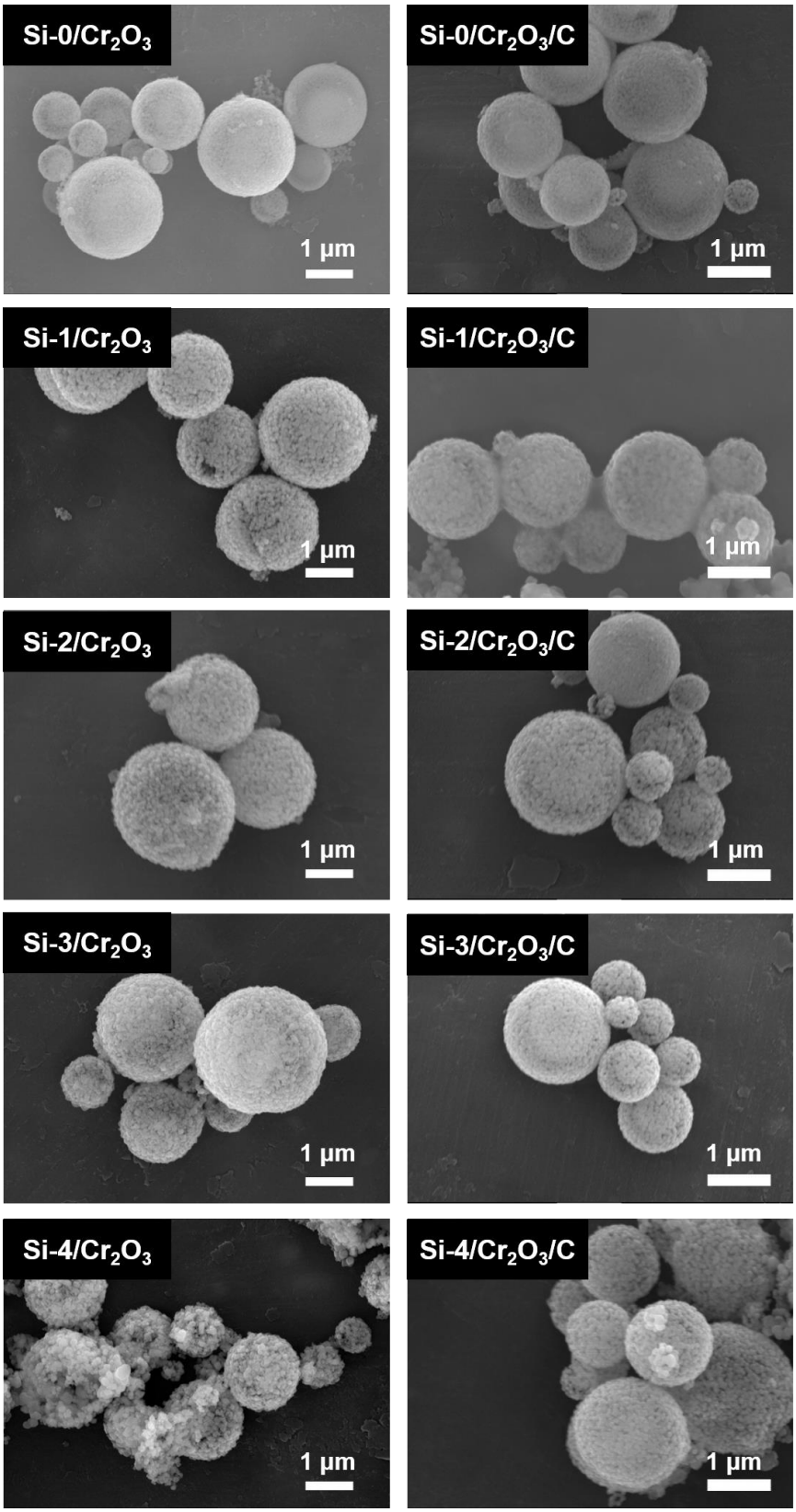

Figure S4 Controlled experiments on Si content. SEM images of the Si/Cr_2O_3 and $Si/Cr_2O_3/C$ samples with different Si contents.

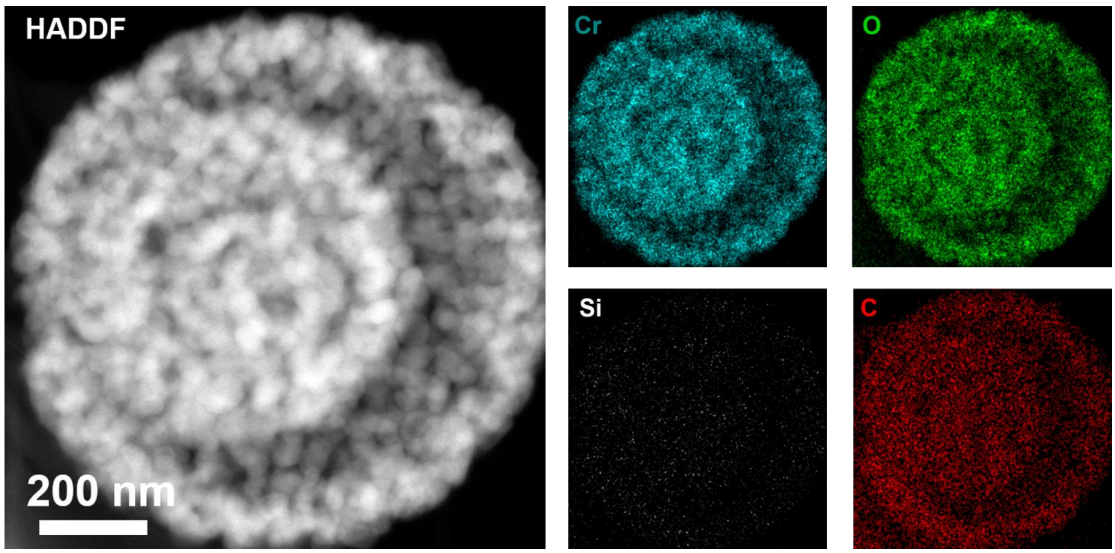

Figure S5 EDS mappings of Cr_2O_3/C. HAADF-STEM images and the corresponding elemental mappings of Cr_2O_3/C.

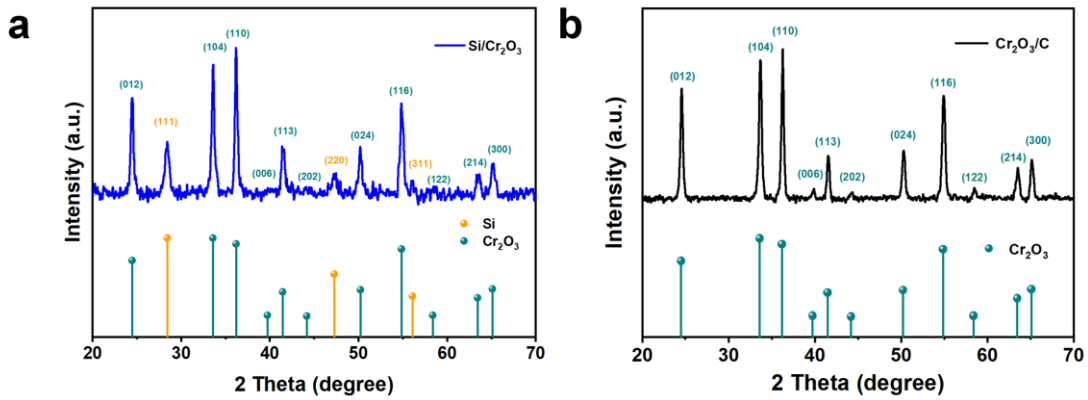

Figure S6 XRD patterns of (a) Si/Cr_2O_3 and (b) Cr_2O_3/C.

Table S2 The crystallite size of Cr_2O_3 determined by the Scherrer equation.

2 Theta (degree)	Diffraction peak	FWHM (degree)	Crystallite size (nm)
24.56217	(012)	0.00557	25.48812
33.68263	(104)	0.00595	24.36893
36.26196	(110)	0.00518	28.20836
54.92642	(116)	0.00712	21.97130

The crystallite size is calculated from the XRD result using the Scherrer equation: $D\text{s}=\frac{k\lambda}{\beta cos\theta}$

where k is the dimensionless particle shape factor associated with crystal geometry/shape (here, k = 0.9 refers to spherical symmetry), λ is the wavelength of Cu Kα X-ray source, β is the full width at half maximum and θ is the Bragg angle.

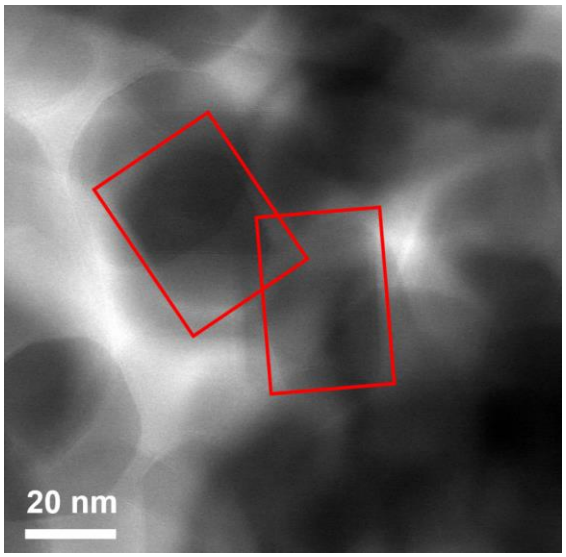

Figure S7 TEM image of Cr_2O_3 showing the particle size.

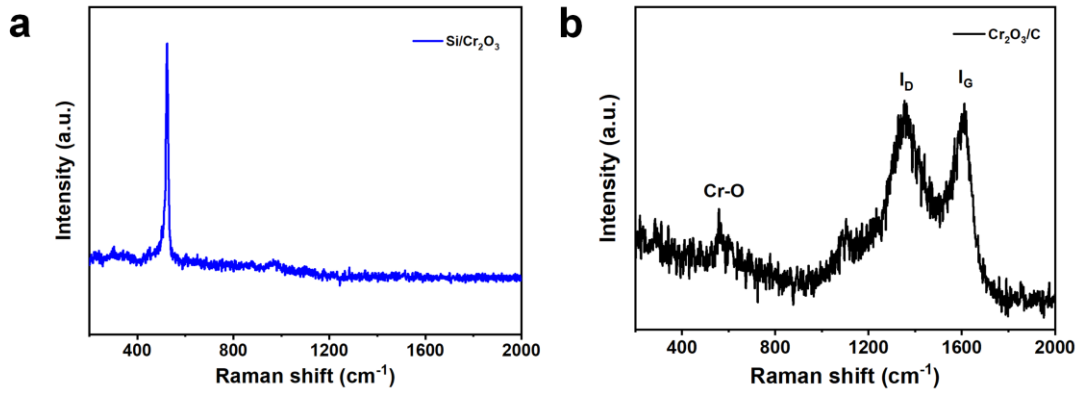

Figure S8 Raman spectra of (a) Si/Cr_2O_3 and (b) Cr_2O_3/C.

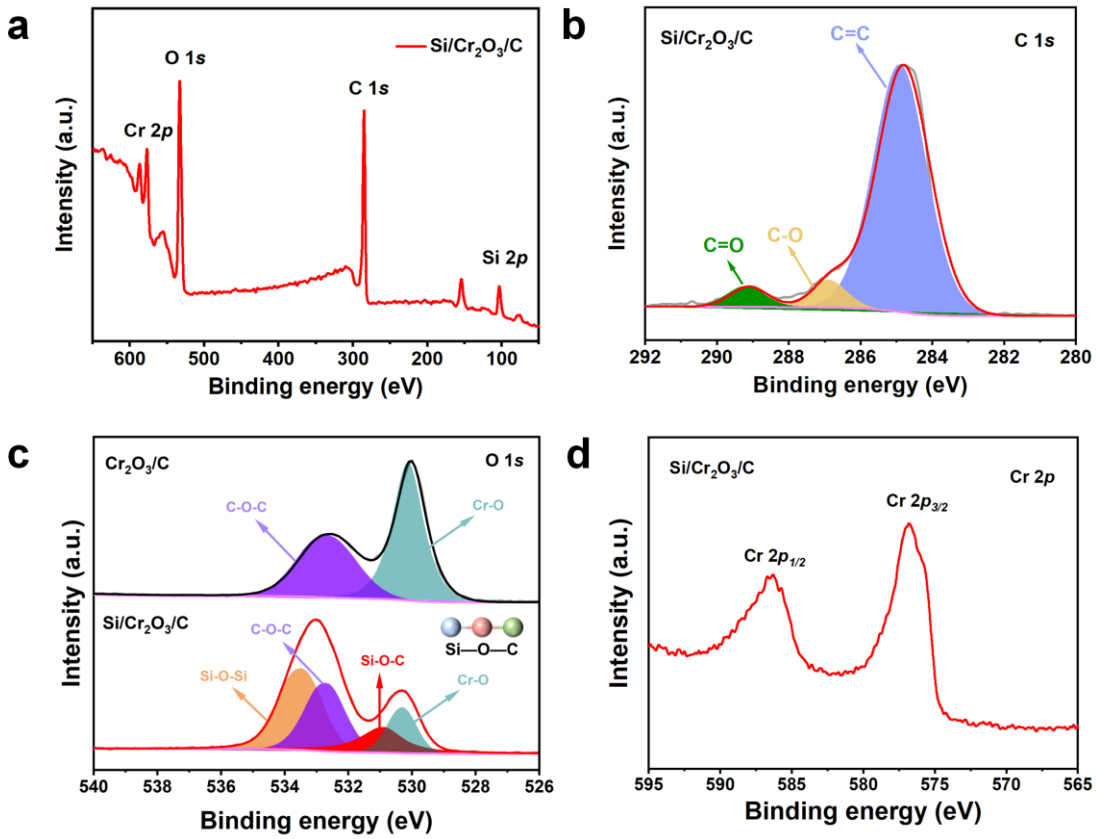

Figure S9 XPS spectra of $Si/Cr_2O_3/C$. (a) XPS survey spectrum of $Si/Cr_2O_3/C$, (b) C 1*s* spectrum of $Si/Cr_2O_3/C$, (c) O 1*s* spectra of $Si/Cr_2O_3/C$ and Cr_2O_3/C, (d) Cr 2*p* spectrum of $Si/Cr_2O_3/C$.

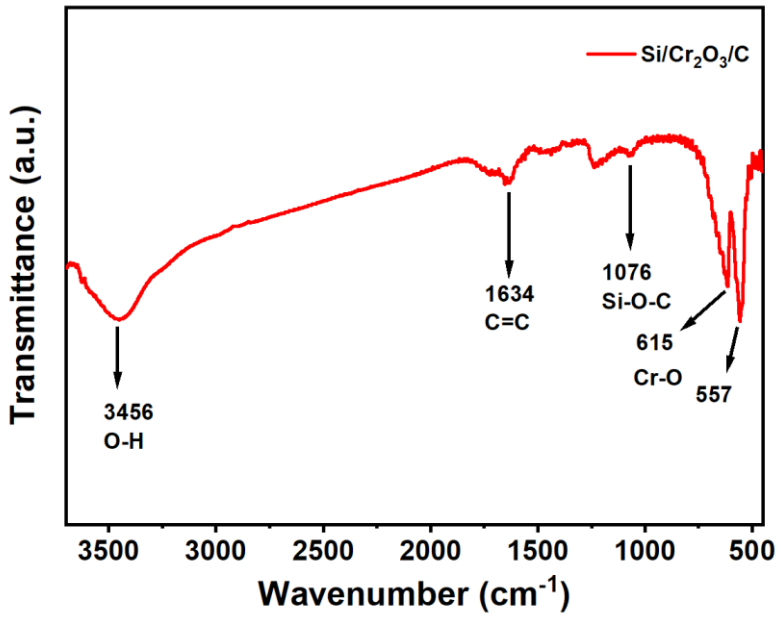

Figure S10 FT-IR spectrum of $Si/Cr_2O_3/C$.

The functional groups on $Si/Cr_2O_3/C$ are analyzed by FT-IR spectrum. The strong peaks at 557 and 615 cm^{-1} are related to symmetric and asymmetric stretching vibrations of the Cr-O band. The peak at 1076 cm^{-1} corresponds to the Si-O-C stretching vibration. The band at 1634 cm^{-1} is related to stretching vibration of C=C derived from acetylene. In addition, the band at 3456 cm^{-1} corresponds to the stretching vibrations of the -OH groups on the surface of the sample.

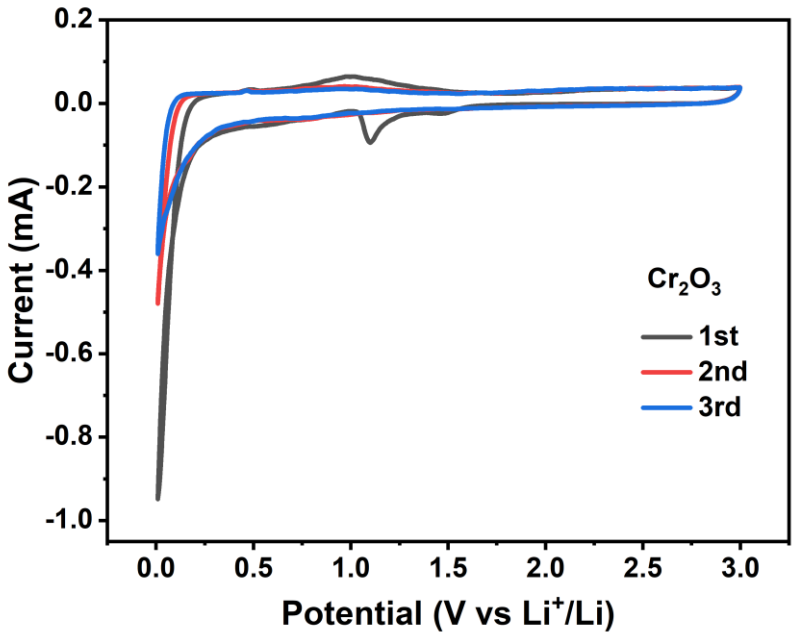

Figure S11 CV profiles of Cr_2O_3.

The cathodic peak at 1.1 V that only appears in the first cycle corresponds to the formation of a SEI film.

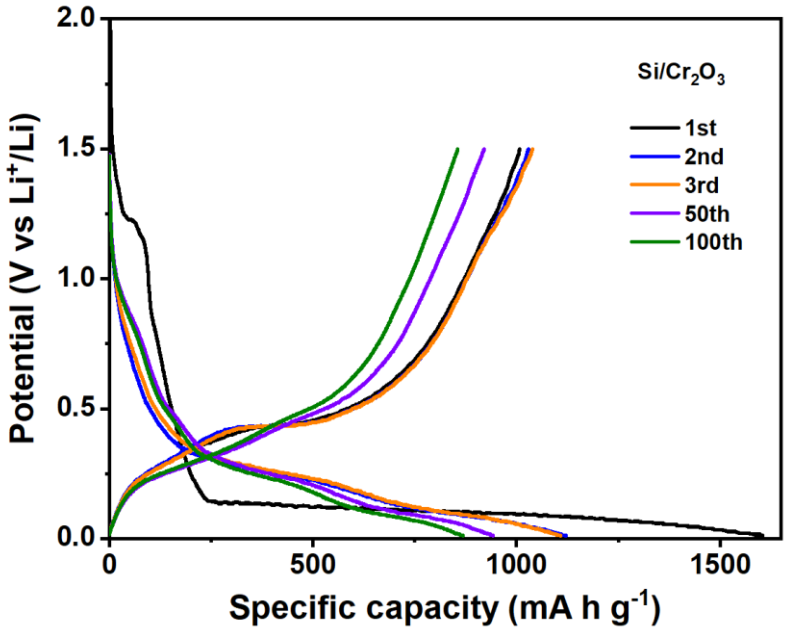

Figure S12 Representative GCD profiles of Si/Cr_2O_3.

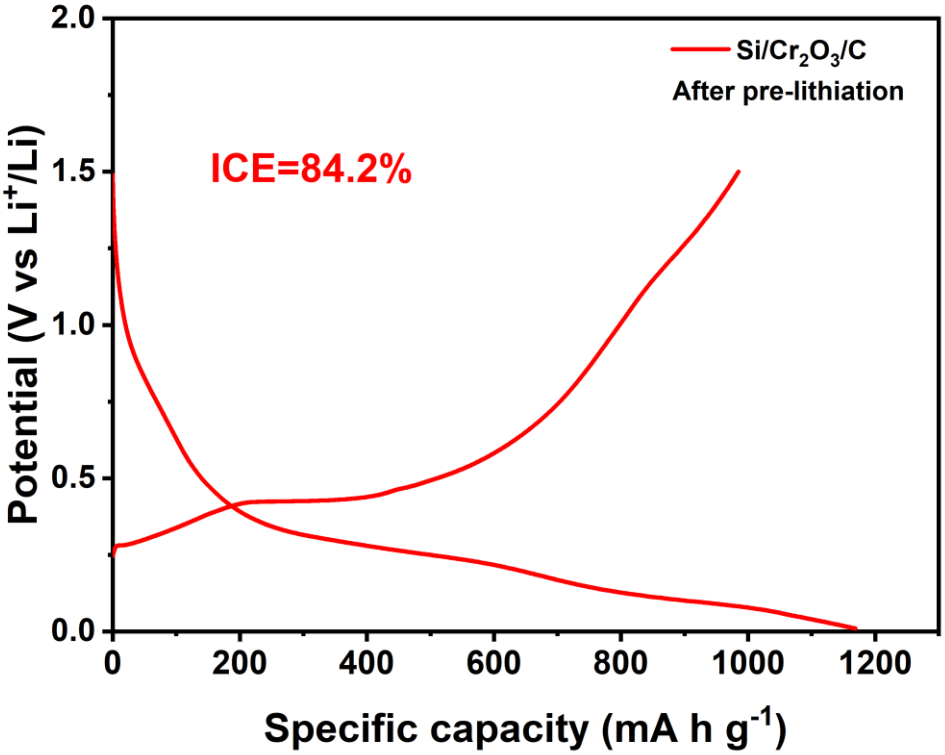

Figure S13 The first-cycle GCD profiles of $Si/Cr_2O_3/C$ after pre-lithiation.

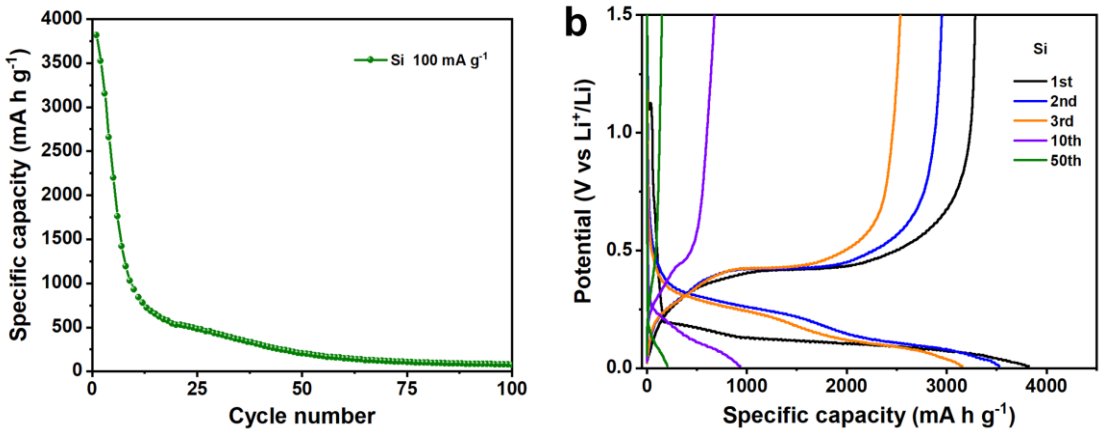

Figure S14 (a) Cycling performance and (b) representative GCD profiles of Si nanoparticles.

The Si nanoparticles exhibit a dramatic capacity fading upon cycling.

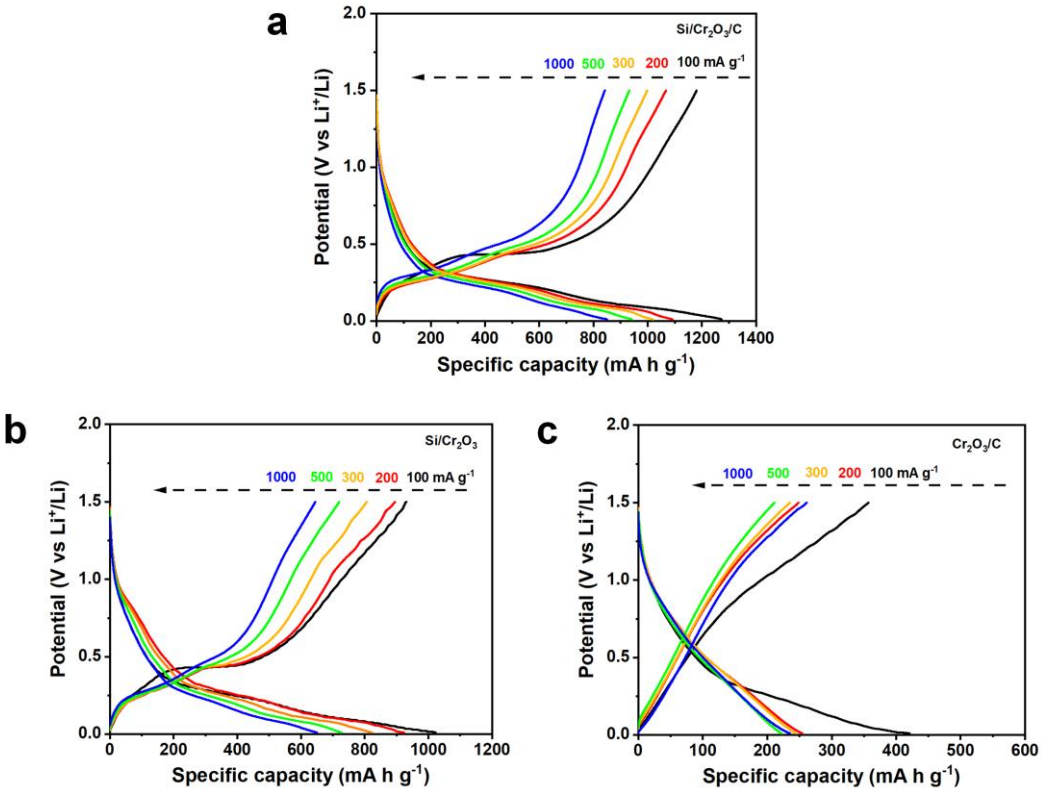

Figure S15 Charge-discharge curves at various current densities. (a) $Si/Cr_2O_3/C$, (b) Si/Cr_2O_3, and (c) Cr_2O_3/C.

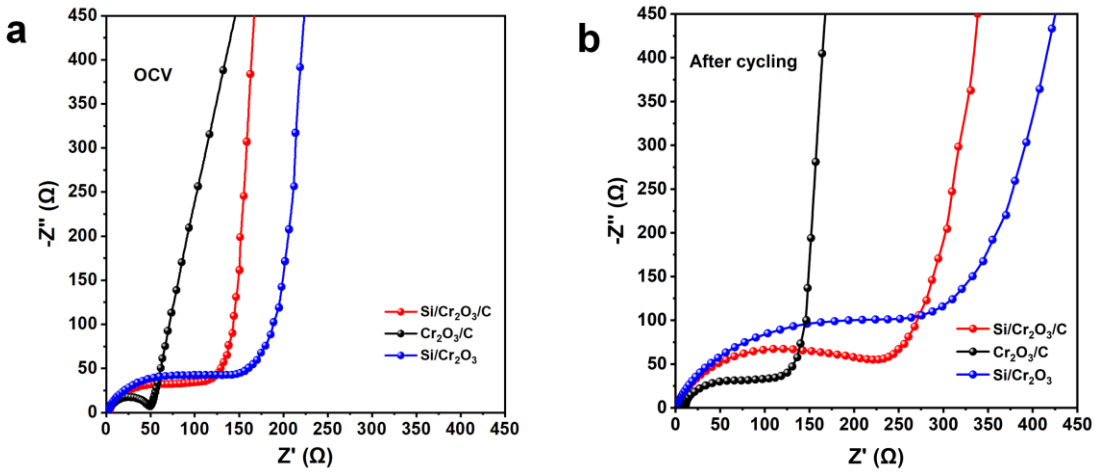

Figure S16 EIS curves of $Si/Cr_2O_3/C$, Si/Cr_2O_3, and Cr_2O_3/C. The Nyquist plots were collected in a frequency range of 0.01 Hz to 100 kHz (a) before cycling and (b) after cycling at 100 mA g^{-1} for 50 cycles.

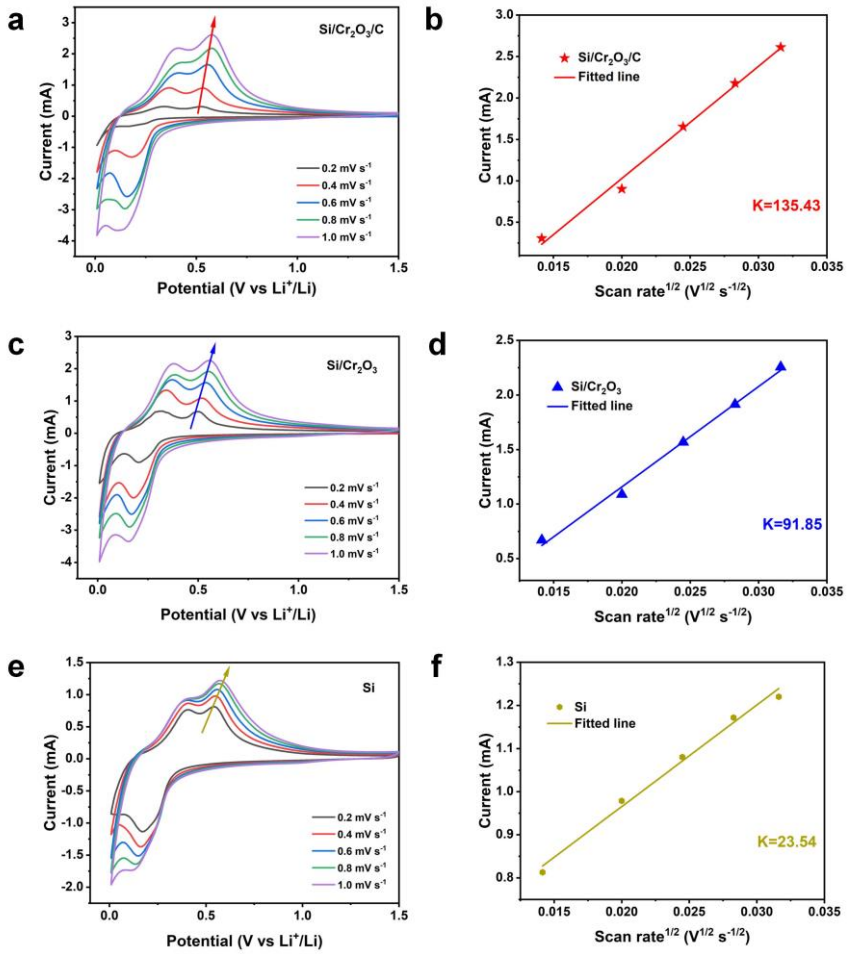

Figure S17 (a, c, e) CV curves ranging from 0.2 to 1.0 mV s^{-1} of $Si/Cr_2O_3/C$, Si/Cr_2O_3, and Si; (b, d, f) relationship between I_p and $\upsilon^{1/2}$.

The Li^+ diffusion coefficient is normally determined by the Randles-Sevcik equation:
$I_p = 2.69 \times 10^5 * n^{3/2} A C_0 D^{1/2} \upsilon^{1/2}$
where the parameters I_p, n, A, C_0, D and υ correspond to peak current, charge-transfer number, electrode surface area, concentration, Li^+ diffusion coefficient, and scan rate, respectively. The highest anodic peaks of Si are chosen to be fitting. The linear relationship between I_p and $\upsilon^{1/2}$ suggests the Li^+ diffusion-dominated reaction kinetics. It should be noted that the Li^+ diffusion coefficient is proportional to the square of slopes (K) as the parameters n, A, and C_0 are similar for $Si/Cr_2O_3/C$, Si/Cr_2O_3, and Si.

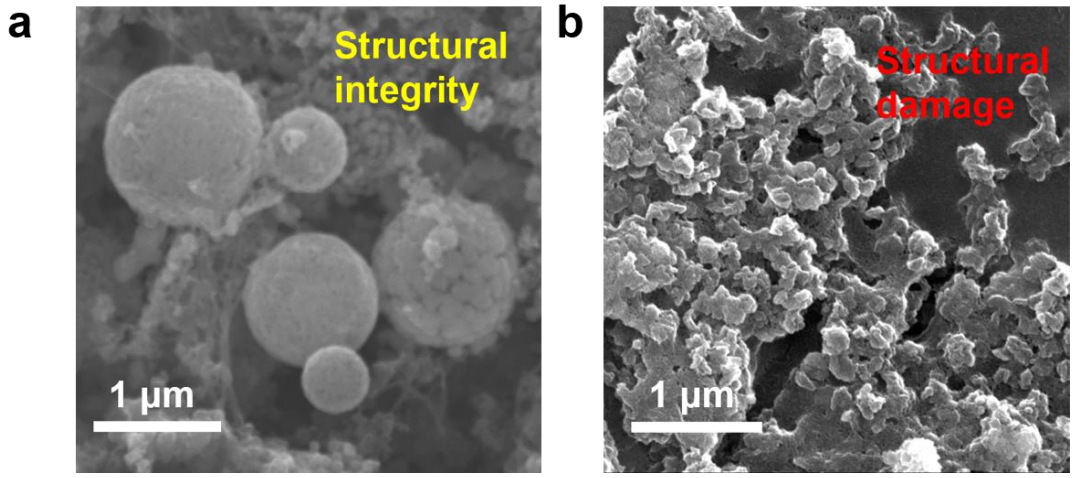

Figure S18 Morphology characterizations after cycling. SEM images of (a) $Si/Cr_2O_3/C$ and (b) Si/Cr_2O_3 after 50 cycles at 100 mA g^{-1}.

The MSHS structure of $Si/Cr_2O_3/C$ is well maintained after 50 cycles, confirming its ideal structural integrity. In contrast, severe pulverization can be observed as for Si/Cr_2O_3.

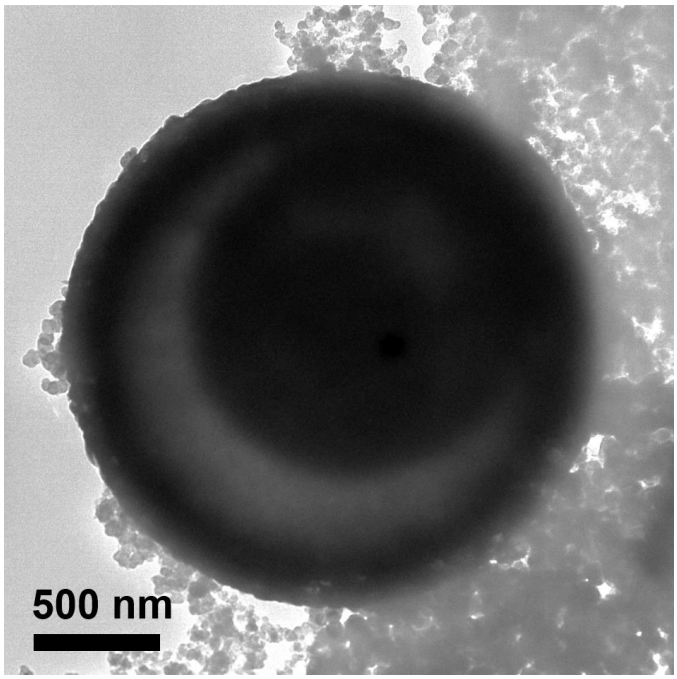

Figure S19 Morphology characterization after cycling. *Ex-situ* TEM image of $Si/Cr_2O_3/C$ after 50 cycles at 100 mA g^{-1}.

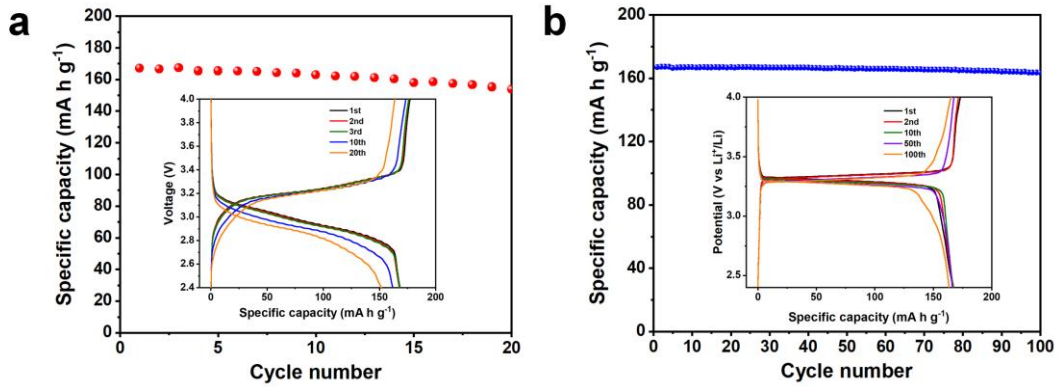

Figure S20 Electrochemical performances of $Si/Cr_2O_3/C//LiFePO_4$ full-cell and $LiFePO_4$. Cycling performances of (a) $Si/Cr_2O_3/C//LiFePO_4$ full-cell and (b) $LiFePO_4$ at 0.1 C with the charge-discharge profiles showing in the inset. The capacity is calculated based on the mass of $LiFePO_4$.

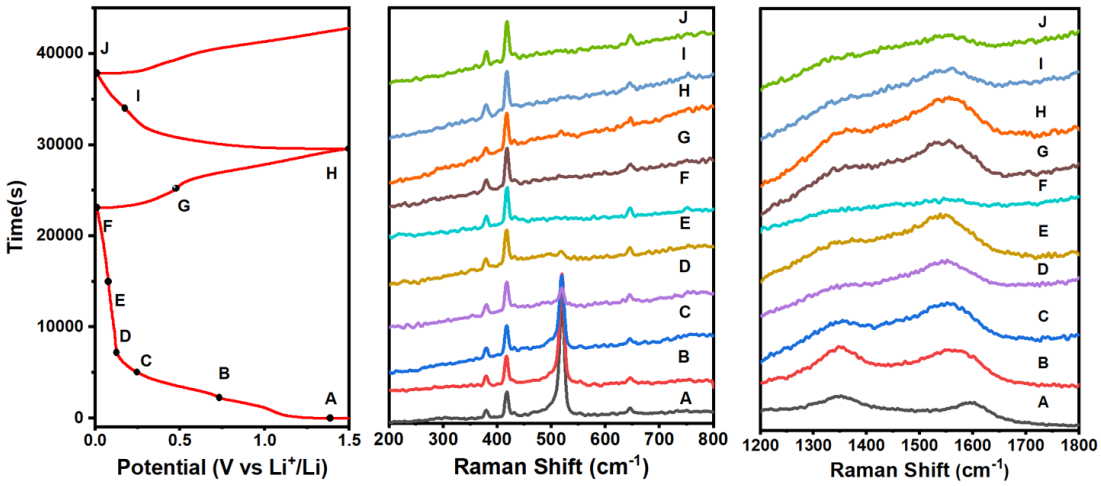

Figure S21 *In-situ* Raman spectra of the Si/Cr_2O_3/C during the first two cycles. The current density for *in-situ* Raman testing is 100 mA g^{-1}.